Article ID: 1000-324X(2018)10-1136-05 **DOI:** 10.15541/jim20170532

Anatase TiO_2 Nanoparticles: Facile Synthesis *via* Non-aqueous Precipitation and Photocatalytic Property

JIANG Feng[1,2], YU Yun[1], FENG Ai-Hu[1,2], YU Yang[1], MI Le[1], SONG Li-Xin[1]

(1. Key Laboratory of Inorganic Coating Materials CAS, Shanghai Institute of Ceramics, Chinese Academy of Sciences, Shanghai 200050, China; 2. University of Chinese Academy of Sciences, Beijing 100049, China)

Abstract: A facile strategy for anatase titanium dioxide (TiO_2) nanoparticle preparation was proposed *via* a non-aqueous precipitation method. With the aid of glacial acetic acid, tetrabutyl titanate underwent non-hydrolytic reaction in solvent ethanol. Glacial acetic acid increased polarity of Ti–O and C–O bonds of tetrabutyl titanate, and promoted non-hydrolytic de-etherization poly condensation reaction to form Ti–O–Ti bond in the solvent. After refluxing at 80℃ for 24 h, the Ti–O–Ti bond was rearranged to form anatase TiO_2 nanoparticles with the particle size of 5 nm-20 nm and specific surface area of 169.4 m^2/g, which exhibited good dispersion and excellent photocatalytic activity. The degradation rate against methyl orange under ultraviolet radiation for 2 h reached 99.81%, showing promising prospect in wastewater treatment process.

Key words: TiO_2; non-aqueous precipitation method; photocatalytic property; low temperature synthesis

TiO_2, a wide band gap semiconductor oxide (E_g= 3.2 eV), has attracted great attention from scientists due to its advantages of good chemical stability, low cost and nontoxicity[1-2]. As a photocatalytic material, TiO_2 and its composite materials show high photocatalytic activity, which can degrade organic pollutants completely into H_2O, CO_2 and other small molecules[3]. It has been confirmed that the crystal structure, particle size and surface characteristics of TiO_2 have great influence on its photocatalytic activity[4-5]. Compared with regular titania, nano TiO_2 has higher surface area and wider light response range, shows more excellent photocatalytic activity[6]. And TiO_2 nano-materials preparation has become the research hotspots in environmental pollution treatment[7-8].

Up to now, several methods have been used to prepare TiO_2 nanomaterials, such as Sol-Gel method[9-10], hydrothermal method[11], precipitation method[12-13], vapor deposition method[14], solid state reaction[15], spray plasma[16], and so on. Among these methods, precipitation method has the superiorities of simple process, low cost, high yield and good quality. However, traditional precipitation method taking water as solvent suffers the problems of sample agglomeration or complicated post-treatment. Non-aqueous precipitation method derives from the traditional precipitation method, which using organic solvent to avoid interference between hydrogen bonds in aqueous system[17-18]. In typical non-aqueous precipitation processes for TiO_2 preparation, titanium tetrachloride reacted with high reactive oxygen donor, *i.e.* tertbutyl alcohol or benzyl alcohol with the promotion of ultrasonic radiation or ultraviolet radiation. But they still had many disadvantages, such as high toxicity, complicate process and serious aggregation of products. Herein, in this work, we show a simple and mild non-aqueous precipitation process for TiO_2 nanoparticles preparation with the aid of glacial acetic acid, which promotes the condensation reaction of tetrabutyl titanate to form TiO_2 nanoparticles at 80℃. The reaction mechanism is discussed, and the photocatalytic performance of as-prepared TiO_2 nanoparticles is also studied.

1 Experiments

1.1 Sample preparation

All reagents and solvents were reagent grade and used without further purification. Tetrabutyl titanate ($Ti(OBu)_4$) was dissolved in 100 mL anhydrous ethanol under stirring at a concentration of 0.284 mol/L. Then, 33 mL glacial acetic acid (AcOH) was added to the solution above. After reflux at 80℃ for 24 h, white precipitate was obtained by non-hydrolytic polycondensation of tetrabutyl titanate with the aid of glacial acetic acid. Subsequently, the white precipitate was separated by centrifugation,

Received date: 2017-11-13; **Modified date:** 2018-06-29
Foundation item: National Natural Science Foundation of China (51162013, 51362014, 51662019)
Biography: JIANG Feng (1990–), male, candidate of PhD. E-mail: 437432167@qq.com
Corresponding author: YU Yun, professor. E-mail: yunyush@mail.sic.ac.cn; SONG Li-Xin, professor. E-mail: lxsong@mail.sic.ac.cn

washed with anhydrous ethanol several times and dried at 80℃ for 2 h. The non-hydrolytic polycondensation by-product was obtained by fractional distilling to centrifugal supernatant, with the removal of ethanol and acetic acid.

1.2 Characterization

X-ray diffraction (XRD, Bruker AXS D8 Advance) with Cu target and *K*a radiation (λ=0.15406 nm) was used for phase identification of the samples. Microstructure was observed by transmission electron microscopy combined with high-resolution (HRTEM, JEM-2000FX). The Brunauer-Emmett-Teller (BET) specific surface area (S_{BET}) was measured by BET isothermal nitrogen adsorption using Micromeritics ASAP 2010 surface area analyzer. Fourier transform infrared (FT-IR) studies were performed by Nicolet 5700 infrared spectrometer within wave number range of 4000 cm^{-1}-400 cm^{-1}.

The degradation of methyl orange ($C_{14}H_{14}N_3NaO_3S$, MO) was carried out in an aqueous solution at room temperature using TiO_2 nanoparticles as catalyzer. Briefly, 0.1 g TiO_2 nanoparticles were added to 50 mL MO solution (10 mg/L) under ultraviolet irradiation (30 W UV lamp with wavelength of 254 nm). After a certain period, the TiO_2 suspension was centrifuged and the concentration of the centrifuged solution was monitored through a wavelength scan on a 721 spectrophotometer (UV-Vis, Shanghai Precision Science Instrument Co Ltd.).

2 Results and discussion

The electron microscopy images of the as-prepared TiO_2 sample are shown in Fig. 1. It is clearly shown in Fig. 1(a) and (b) that the sample has irregular shape with the particle size of 5 nm-20 nm. According to HRTEM image in Fig. 1(c), the interplanar spacing is about 0.35 nm, which is close to the (101) spacing of anatase TiO_2. And Fig. 1(d) clearly shows that TiO_2 sample has polycrystalline diffraction rings structure.

Fig. 2 shows the infrared spectra of samples at different stages of the preparation process, including $Ti(OBu)_4$, mixture of $Ti(OBu)_4$ and AcOH, precipite slurry and precipitate. Table 1 lists the corresponding attribution of major bonds in infrared spectra.

Compared with the IR spectrum of $Ti(OBu)_4$, new bands at 1724 cm^{-1}, 1547 cm^{-1}, 1290 cm^{-1} and 1070 cm^{-1} related to the COO stretching vibration appear in the spectrum of the mixture , while the bands at 1124 cm^{-1}-1039 cm^{-1} attributed to the Ti–O–C stretching vibration disappear. More importantly, the bands at 1028 cm^{-1} and 611 cm^{-1} assigned to C–O and Ti–O vibration exhibit

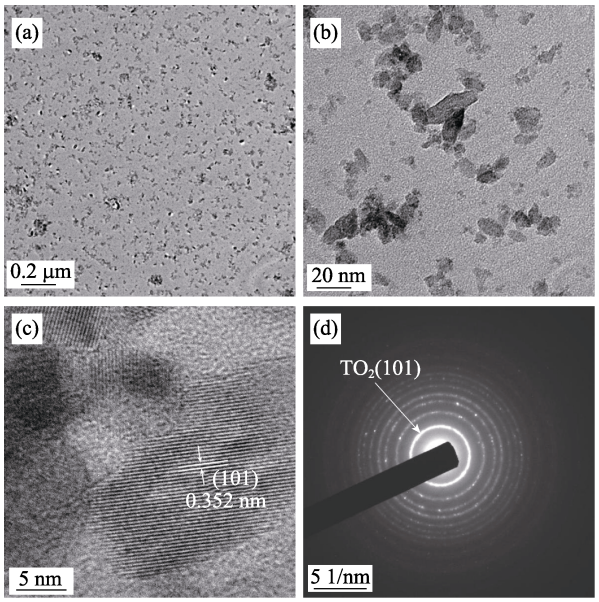

Fig. 1　(a, b) TEM, (c) HRTEM images and (d) SAED pattern of the as-prepared TiO_2 nanoparticles

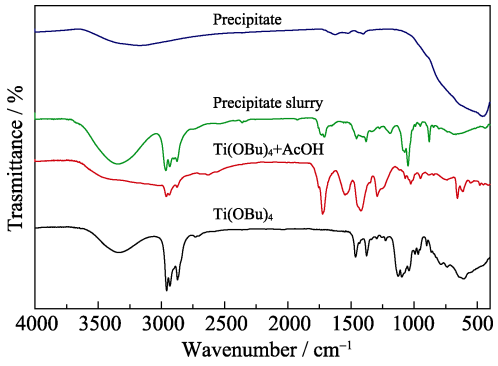

Fig. 2　FT-IR spectra of samples at different reaction stages

red shifts to 1045 cm^{-1} and 613 cm^{-1}, respectively. It should be noted that the peak of OH bond in glacial acetic acid is not observed in the mixture. The results clearly demonstrate that the AcOH has coordinated with $Ti(OBu)_4$, which changes the characteristic structure of the Ti–O–C group in $Ti(OBu)_4$, and the OH group of glacial acetic acid disappears simultaneously.

Therefore, a probable chemical reaction for above process is shown in Fig. 3. The H atom at position 1 coordinates with RO (R=Bu) in tetrabutyl titanate to form hydrogen bond. The electron-withdrawing inductive effect of H atom can greatly reduce the charge density of O in the titanium alkoxide, and then weaken the bond strength of the Ti–O bond as well as the C–O bond. This process also increases the polarity of above two bonds, resulting in the red shift of the infrared peak position.

From the IR spectrum of precipitate slurry, it can be clearly seen that Ti–O–Ti bond appears at 438 cm^{-1}, which is mainly generated from the attacking of RO

Table 1 Peak position of samples at different reaction stages (cm^{-1})

$Ti(OBu)_4$	$Ti(OBu)_4$ + AcOH	Precipitate slurry	Precipitate	Attribution	Ref.
3334	–	3334	–	OH	[19]
2958	2958	2958	–	C–H	[20]
2933	2933	2933	–	aromatic C–C	[21]
2873	2873	2873	–	C–H	[20]
2700	–	–	–	C–H	[20]
1460	–	–	–	$–CH_2$	[22]
1379	1419	–	–	$–CH_3$	[22]
1124	–	–	–	Ti–O–C	[23]
1096	–	–	–	Ti–O–C	[23]
1039	–	–	–	Ti–O–C–	[23]
611	613	–	–	Ti–O	[24]
–	1724	1735	–	–C═O	[25]
–	1547	–	–	COO-group	[26]
–	1290	–	–	C–O	[27]
–	1070	1074	–	C–O	[28]
–	1028	1045	–	C–O	[29]
–	–	1458	–	CH_2	[30]
–	–	1378	–	Sym COO	[31]
–	–	1189	–	C–O	[32]
–	–	881	–	C–COO	[31]
–	–	438	455	Ti–O–Ti	[33]

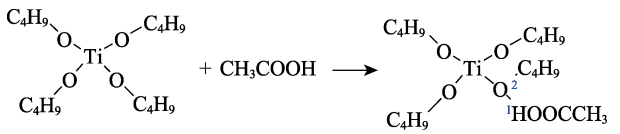

Fig. 3 Mechanism of acetic acid coordinated with butyl titanate

group to the alkyl R in another $Ti(OBu)_4$ molecule with the formation of BuOBu simultaneously. BuOBu is demonstrated by the FT-IR spectrum of the non-hydrolytic polycondensation by-product, as shown in Fig. 4. The appearance of C–O–C bond at 1120 cm^{-1}[34] indicates the formation of BuOBu. Moreover, there are not any other peaks except Ti–O–Ti bond in the FT-IR spectrum of precipitate, indicating the non-hydrolytic polycondensation reaction is complete.

Based on the above results, a schematic diagram mechanism for the formation of TiO_2 nanoparticles is presented in Fig. 5. Briefly, the hydrogen atom in hydroxyl group of AcOH (position 1) coordinates with oxygen atom in $Ti(OBu)_4$ (position 2) to form the hydrogen bond, which causes the weakness of the Ti–O and C–O bonds. Therefore, it contributes to the formation of Ti–O–Ti bond through the non-hydrolytic polycondensation process. After refluxing, the anatase TiO_2 nanoparticles form through the rearrangement of Ti–O–Ti network.

The photocatalytic activities of as-prepared TiO_2 sample and P25 were studied and measurements were performed by the photo degradation of MO under UV light. The results are shown in Fig. 6(a, b), respectively. The characteristic absorption of MO at 464 nm is chosen to monitor its concentration. It is obvious that the main

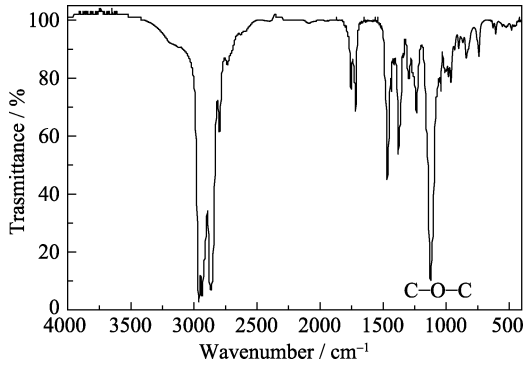

Fig. 4 FT-IR spectrum of the non-hydrolytic polycondensation by-product

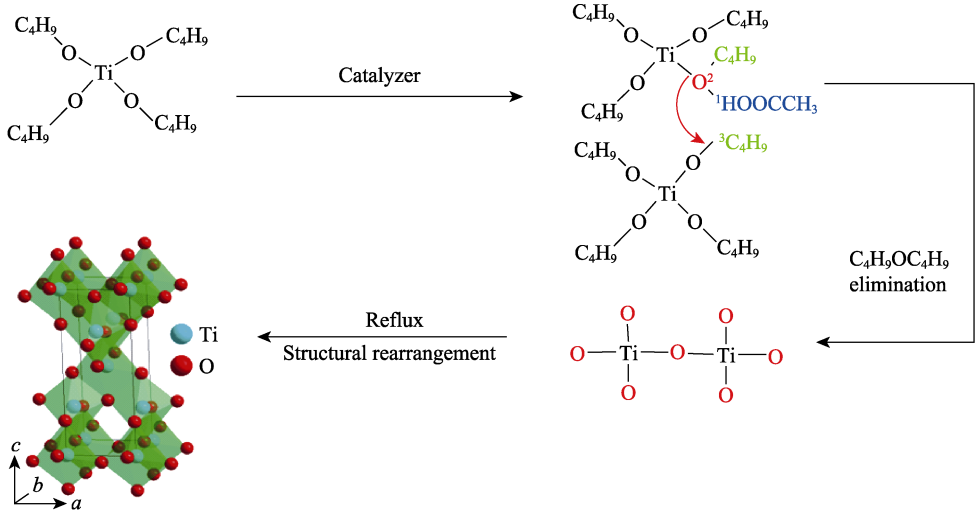

Fig. 5 Schematic diagram of the proposed mechanism for the formation of TiO_2 nanoparticles

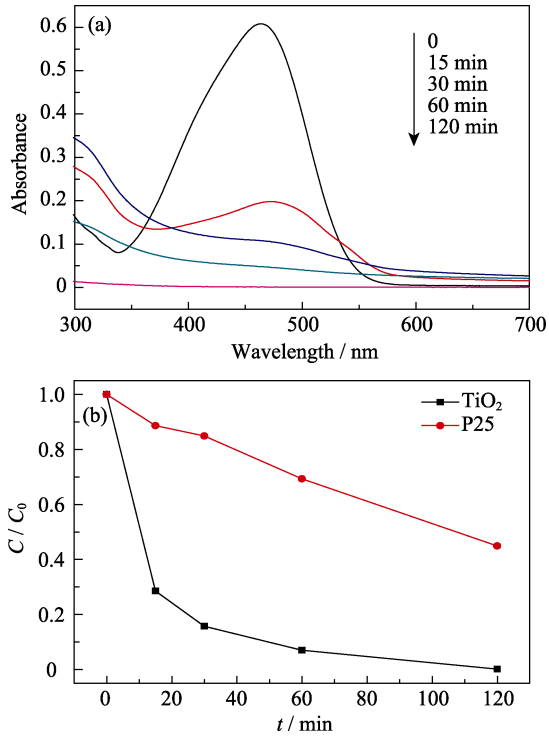

Fig. 6　Photodegradation effect of TiO_2 nanoparticles
(a) UV-Vis absorption spectra of MO solutions after photocatalytic performance test at different time intervals; (b) Photodegradation rate of MO after photocatalysis by TiO_2 nanoparticles and commercial P25 powders

absorption peak has basically disappeared after 60 min, indicating the anatase TiO_2 nanoparticles have a high degradation activity due to their large surface area. After irradiation for 120 min, the anatase TiO_2 nanoparticles remove about 99.81% of MO. In comparison, commercial P25 powders with the surface area of 37.0 m^2/g are employed to remove MO, and their degradation rate is only 55.06% after 120 min, which is much lower than that of as-prepared TiO_2. This is mainly because the large surface area of as-prepared TiO_2 sample (169.4 m^2/g) might benefit the photocatalytic degradation of MO.

Furthermore, photocatalytic reactions can be expressed by the Langmuir-Hinshelwood (L-H) model[35]. The photo degradation of MO obeys pseudo-first order kinetics as compared to the initial concentration of MO:

$$\ln(c_t/c_0) = -Kt + C \quad (1)$$

Where, c_0 and c_t are the initial and final MO concentration, at time t=0 and t=t respectively. K is the reaction rate constant, which is the slope of the plot $-\ln(c_t/c_0)$ *versus* time.

Fig. 7 shows the $\ln(c_t/c_0)$ –t curves of samples. And the photocatalytic degradation rate constant for as-prepared TiO_2 and P25 under UV light was found to be 2.68×10^{-2} min^{-1} and 3.1×10^{-3} min^{-1}, respectively. Thus, as-prepared TiO_2 is considered to possess superior photo degradation ability, and it can be an ideal candidate for pollution treatment.

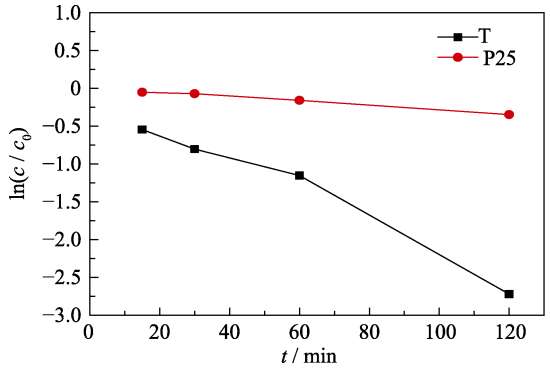

Fig. 7　Kinetics of MO photodegradation (linear transform $\ln(c/c_0)$ *vs* t in photocatalytic experiments)

3　Conclusion

In summary, anatase TiO_2 nanoparticles were prepared *via* a facile non-aqueous precipitation method at low temperature in anhydrous ethanol solvent. The glacial acetic acid can increase the polarity of Ti–O bond and C–O bond in tetrabutyl titanate, while promote the non-hydrolytic de-etherization polycondensation reaction. The as-prepared TiO_2 nanoparticles exhibit high dispersion with the particle size range of 5 nm-20 nm and a specific surface area of 169.4 m^2/g. All data demonstrate that the TiO_2 nanoparticles have excellent degradation performance to methyl orange, making it a promising candidate for wastewater treatment.

References:

[1] KHAN S U M, AL S M, INGLER W B. Efficient photochemical water splitting by a chemically modified *n*-TiO_2. *Science*, 2002, **297(5590):** 2243–2245.
[2] BACH U, LUPO D, COMTE P, *et al*. Solid-state dye-sensitized mesoporous TiO_2 solar cells with high photon-to-electroncon-version efficiencies. *Nature*, 1998, **395(6702):** 583–585.
[3] GAYA U I, ABDULLAH A H. Heterogeneous photocatalytic degradation of organic contaminants over titanium dioxide: a review of fundamentals, progress and problems. *Journal of Photochemistry & Photobiology C Photochemistry Reviews*, 2006, **9(1):** 1–12.
[4] JUNG K Y, PARK S B, JANG H D. Phase control and photocatalytic properties of nano-sized titania particles by gas-phase pyrolysis of $TiCl_4$. *Catalysis Communications*, 2004, **5(9):** 491–497.
[5] LOOK J L, ZUKOSKI C F. Alkoxide-derived titania particles: use of electrolytes to control size and agglomeration levels. *Journal of the American Ceramic Society*, 2010, **75(6):** 1587–1595.
[6] JIANG H Q, WANG P, GUO X L, *et al*. Preparation and characterization of low-amount Yb^{3+}-doped TiO_2 photocatalyst. *Russian Chemical Bulletin*, 2006, **55(10):** 1743–1747.
[7] GUO Y G, HU Y S, SIGLE W. Superior electrode performance of nanostructured mesoporous TiO_2 (anatase) through efficient hierarchical mixed conducting networks. *Advanced Materials*, 2007, **19(16):** 2087–2091.
[8] ADDAMO M, AUGUGLIARO V, PAOLA A D, *et al*. Preparation, characterization, and photoactivity of polycrystalline nanostructured TiO_2 catalysts. *The Journal of Physical Chemistry A*, 2004, **35(21):** 3303–3310.
[9] SUGIMOTO T, ZHOU X, MURAMATSU A. Synthesis of uniform

anatase TiO_2 nanoparticles by Gel-Sol method 4. Shape control. *Journal of Colloid and Interface Science*, 2003, **259(1):** 53–61.
[10] SUGIMOTO T, ZHOU X, MURAMATSU A. Synthesis of uniform anatase TiO_2 nanoparticles by Gel-Sol method. 3. Formation process and size control. *Journal of Colloid and Interface Science*, 2003, **259(1):** 43–52.
[11] ZHANG Y X, LI G H, JIN Y X. Hydrothermal synthesis and photoluminescence of TiO_2 nanowires. *Chemical Physics Letters*, 2002, **365(3/4):** 300–304.
[12] HE W, FANG Z, ZHANG K, *et al*. Continuous synthesis of a co-doped TiO_2 photocatalyst and its enhanced visible light catalytic activity using a photocatalysis microreactor. *RSC Advances*, 2015, **5(68):** 54853–54860.
[13] REYES C D, RODRÍGUEZ G G, ESPINOSA P M E, *et al*. Phase-pure TiO_2 nanoparticles: anatase, brookite and rutile. *Nanotechnology*, 2008, **19(14):** 1–10.
[14] CHAN S K, KOICHI N, BIN X, *et al*. A new observation on the phase transformation of TiO_2 nanoparticles produced by a CVD method. *Aerosol Science & Technology*, 2005, **39(2):** 104–112.
[15] FENG Q, WANG T, ZHANG F, *et al*. Synthesis of TiO_2 photocatalytic materials *via* solid-state reaction and its photodegradation property for methyl orange. *Material Research Innovations*, 2015, **18(S4):** 92 –96.
[16] BANNIER E, DARUT G, SÁNCHEZ E, *et al*. Microstructure and photocatalytic activity of suspension plasma sprayed TiO_2 coatings on steel and glass substrates. *Surface & Coatings Technology*, 2011, **206(2/3):** 378–386.
[17] ZHU J, BIAN Z F, REN J, *et al*. An integrated low temperature approach to highly photoactive nanocrystalline mesostructured titania. *Catalysis Communications*, 2007, **8(7):** 971–976.
[18] ZHU J, YANG J, BIAN Z F, *et al*. Nanocrystalline anatase TiO_2 photocatalysts prepared *via* a facile low temperature nonhydrolytic Sol–Gel reaction of $TiCl_4$ and benzyl alcohol. *Applied Catalysis B Environmental*, 2007, **76(1):** 82–91.
[19] PIRES D C, STOCKLERPINTO D V B, SCIAMARELI J, *et al*. Synthesis and characterization by infrared spectroscopy of hydantoin-based bonding agents, used in composite propellants. *Journal of Aerospace Technology & Management*, 2009, **1(2):** 177–184.
[20] MAX J J, DANEAULT S, CHAPADOS C. 1-Propanol hydrate by IR spectroscopy. *Canadian Journal of Chemistry*, 2002, **80(1):** 113–123.
[21] JULKAPLI N M, AHMAD Z, AKIL H M. Preparation and characterization of 1,2,4,5-benzenetetra carboxylic-chitosan. *E-Polymers*, 2010, **10(1):** 841–857.
[22] ENESCU D, FRACHE A. Effects of sterically hindered *N*-alkoxyamines on photooxidative stability of reinforced polypropylene. *E-Polymers*, 2013, **12(1):** 949–959.
[23] VELASCO M J, RUBIO F, RUBIO J. Hydrolysis of titanium tetrabutoxide. study by FT-IR spectroscopy. *Spectroscopy Letters*, 1999, **32(2):** 289–304.
[24] HWANG J D, CHOU C H. On the origin of leakage current reduction in TiO_2 passivated porosus silicon Schottky-barrier diode. *Applied Physics Letters*, 2010, **96(6):** 063501–063503.
[25] URBAN M W, KOENIG J L, SHIH L B, *et al*. Structure of styrene/acrylic acid copolymer in aqueous solution determined by Fourier transform infrared spectroscopy. *Applied Spectroscopy*, 1987, **41(4):** 590–596.
[26] FUGU M B, NDAHI N P, PAUL B B, *et al*. Synthesis, characterization, and antimicrobial studies of some vanillin schiff base metal (ii) complexes. *Journal of Chemical & Pharmaceutical Research*, 2013, **5(1):** 22–28.
[27] ZHANG W, ZHANG H, XIAO J, *et al*. Carbon nanotube catalyst for oxidative desulfurization of a model diesel fuel using molecular oxygen. *Green Chemistry*, 2013, **16(1):** 211–220.
[28] GEIGER C, ZELENKA C, WEIGL M, *et al*. Synthesis of bicyclic sigma receptor ligands with cytotoxic activity. *Journal of Medicinal Chemistry*, 2007, **50(24):** 6144–6153.
[29] SUN S L, WEN J L, MA M G, *et al*. Successive alkali extraction and structural characterization of hemicelluloses from sweet sorghum stem. *Carbohydr. Polym.*, 2013, **92(2):** 2224–2231.
[30] NIKODEM K, GRAŻYNA S G, LIDIA O, *et al*. A study on the synthesis and properties of substituted EHBG-Fe(iii) complexes as potential MRI contrast agents. *Journal of Organometallic Chemistry*, 2014, **769(1):** 100–105.
[31] CHOE J I, KIM G H. *Ab initio* study of vibrational spectra of *p*-tert-butylcalix[4]aryl ester complexed with alkali metal cation. *Journal of the Korean Chemical Society*, 2006, **50(1):** 7–13.
[32] SUGIHARTO A B, JOHNSON C M, DUNLOP I E, *et al*. Delocalized surface modes reveal three-dimensional structures of complex biomolecules. *Journal of Physical Chemistry C*, 2008, **112(20):** 7531–7534.
[33] LI Z, HOU B, XU Y, *et al*. Comparative study of Sol–Gel-hydrothermal and Sol–Gel synthesis of titania–silica composite nanoparticles. *Journal of Solid State Chemistry*, 2005, **178(5):** 1395–1405.
[34] LIANG C Y, KRIMM S. Infrared spectra of high polymers: Part IX. Polyethylene terephthalate. *Journal of Molecular Spectroscopy*, 1959, **3(1–6):** 554–574.
[35] ZHANG L, LI H, LIU Y, *et al*. Adsorption-photocatalytic degradation of methyl orange over a facile one-step hydrothermally synthesized TiO_2/ZnO-NH_2-RGO nanocomposite. *RSC Advances*, 2014, **4(89):** 48703–48711.

非水沉淀法制备纳米氧化钛及其光催化性能研究

江 峰[1,2], 于 云[2], 冯爱虎[1,2], 于 洋[1], 米 乐[1], 宋力昕[1]

(1 中国科学院 上海硅酸盐研究所, 中国科学院特种无机涂层重点实验室, 上海 200050; 2. 中国科学院大学, 北京 100049)

摘 要: 采用非水沉淀工艺制备了锐钛矿型纳米氧化钛(TiO_2)。在冰醋酸的催化作用下, 钛酸丁酯在乙醇中发生非水解反应。冰醋酸的引入增加了钛酸丁酯中 Ti–O 键和 C–O 键的极性, 进而促进其在溶剂乙醇中发生非水解脱醚缩聚反应形成 Ti–O–Ti 键合。经过 80℃回流 24 h, Ti–O–Ti 键重排形成锐钛矿型纳米 TiO_2。其粒径为 5~20 nm; 比表面积为 169.4 m^2/g。非水沉淀法制备的纳米氧化钛分散性良好, 光催化性能优异。紫外光照 2 h, 纳米氧化钛对甲基橙的降解率达 99.81%, 具有良好的污水处理应用前景。

关 键 词: TiO_2; 非水沉淀法; 光催化性能; 低温合成

中图分类号: TQ174 **文献标识码:** A